Motion Artifacts of Pulse Inversion-Based Tissue Harmonic Imaging

Che-Chou Shen and Pai-Chi Li, *Senior Member, IEEE*

Abstract—**Motion artifacts of the pulse inversion technique were studied for finite amplitude distortion-based harmonic imaging. Motion in both the axial and the lateral directions was considered. Two performance issues were investigated. One is the harmonic signal intensity relative to the fundamental intensity and the other is the potential image quality degradation resulting from spectral leakage. A one-dimensional (1-D) correlation-based correction scheme also was used to compensate for motion artifacts. Results indicated that the tissue harmonic signal is significantly affected by tissue motion. For axial motion, the tissue harmonic intensity decreases much more rapidly than with lateral motion. The fundamental signal increases for both axial and lateral motion. Thus, filtering is still required to remove the fundamental signal, even if the pulse inversion technique is applied. The motion also potentially decreases contrast resolution because of the uncancelled spectral leakage. Also, it was indicated that 1-D motion correction is not adequate if nonaxial motion is present.**

I. Introduction

Tissue harmonic imaging has the ability to improve contrast resolution over conventional fundamental imaging [1]–[3]. It has become an important diagnostic tool in many clinical applications [4]. The tissue harmonic signal is generated by finite amplitude distortion of a propagating sound wave, and the harmonics are generated at frequencies that are multiples of the transmit frequency [5]–[7]. Conventionally, the tissue harmonic signal is extracted from the received echo by band-pass or high-pass filtering. Although filtering can be efficiently implemented, it also suffers from potential contrast degradation resulting from spectral leakage [8]. In other words, non-negligible harmonic components may have been present at the surface of the transducer prior to propagation if the pulse bandwidth is large or the ultrasound system itself is nonlinear. Such a leakage signal propagates linearly and combines with the tissue harmonic signal. The leakage signal cannot be filtered out from the tissue harmonic signal due to the spectral overlap of the two signals, and it potentially degrades the contrast resolution in tissue harmonic imaging.

The pulse inversion (PI) technique is an alternative method to extract the tissue harmonic signal [9], [10]. In this case, two transmissions are required for each acoustic beam line. After a pulse is transmitted in the first firing, the same pulse is inverted and transmitted again in the second firing. The echoes in both firings are summed together to obtain a beam. Because an inverted pulse is the original pulse with 180° phase shift, the method also is known as the phase-inversion technique [11]. In the sum signal, the linearly propagated signal is cancelled and only nonlinearly generated components remain. Thus, a better fundamental signal cancellation is expected with the PI technique. In addition, the contrast resolution can be improved as spectral leakage is completely cancelled [8]. Nonetheless, the PI technique requires twice the data acquisition time compared to the conventional filtering approach. In other words, it suffers from frame rate reduction and potential motion artifacts. In clinical situations, motion artifacts of the PI technique result from the relative movement between the probe and the imaged tissue during the two firings. With motion, the linearly propagating signal is not completely cancelled, and the harmonic intensity becomes smaller due to signal misalignment. In addition, the frequency range of the uncancelled linear signal also may overlap with the tissue harmonic signal and results in image degradation. It is the primary purpose of this paper to investigate such potential motion artifacts of the PI technique in tissue harmonic imaging.

In Section II, both the fundamental signal intensity and the harmonic signal intensity are investigated using simulations and experiments when tissue motion is present. In Section III, acoustic radiation patterns are simulated and experimentally measured to investigate the motion effects on the sidelobe level. B-scan images also are constructed to demonstrate the potential image quality degradation. The paper concludes in Section IV with a discussion on the motion artifacts of other imaging pulse sequences. Feasibility of motion correction is also studied.

II. Motion Effects on Signal Intensity

In this section, motion effects on both the fundamental and the harmonic signal intensity are investigated using simulations and experiments. The simulation model used is similar to the one used by Christopher [1] and Li and Shen [3]. The transmit waveform is first decomposed into discrete temporal frequency components. For each frequency component, continuous beam formation is approximated by incremental field propagation. At each increment, linear propagation is simulated based on the angular spectrum

Manuscript received January 10, 2002; accepted April 9, 2002. Support partially supplied from the National Science Council of R.O.C. under Grant NSC 90-2213-E-002-127, and partially from National Health Research Institute of R.O.C., is gratefully acknowledged.

The authors are with the Department of Electrical Engineering, National Taiwan University, Taipei, Taiwan 106, R.O.C. (e-mail: paichi@cc.ee.ntu.edu.tw).

method [12], [13]. The nonlinear propagation is modeled using the finite amplitude distortion model [14]. As shown in the following equation, the finite amplitude distortion model utilizes the frequency domain solution to Burgers' equation, i.e.,

$$u_n = u'_n + j\frac{\beta\pi f\Delta z}{2c^2}\left[\sum_{k=1}^{n-1} k u'_k u'_{n-k} + \sum_{k=n}^{N} n u'_k u'^{*}_{k-n}\right] \quad (1)$$

In (1), Δz is the propagation increment along the axial direction. The fundamental frequency is denoted by f and β is a parameter representing the nonlinearity of the propagating medium. The term u'_n denotes the temporal velocity field at frequency nf (n is an integer) after linear propagation. Likewise, u_n denotes the temporal velocity field after nonlinear propagation. The sound velocity is denoted by c.

A 1-D linear array with 96 channels was simulated. The array had a 0.3 mm pitch and the transmit focus was set to 55 mm away from the transducer. The transmit signal was a 2 MHz Gaussian pulse with a -6 dB 50% fractional bandwidth. The smooth Gaussian envelope produces less spectral leakage than envelopes with sharp edges. The propagating medium was homogeneous and the nonlinear parameter β was 3.5, approximating the nonlinear property of water [15]. To obtain the sum signal in the PI technique, two simulations were performed to acquire sound fields corresponding to the positive and the negative pulses. The sound field generated by the positive pulse interacted with the imaged tissue at an original position. Based on the tissue velocity and the pulse repetition interval (PRI), the new position of the target was found and the sound field generated by the negative pulse was calculated. The imaged object is first assumed to be a single scatterer positioned in the focal point and the motion artifacts are investigated separately in the axial direction and in the lateral direction.

Fig. 1 demonstrates the simulation results with axial motion. The horizontal axis is the axial displacement (d_{axial}) normalized to the wavelength at the fundamental frequency (λ) and the displacement is assumed to be sufficiently small compared to the duration of the pulse envelope. With no displacement, Fig. 1 shows that the second harmonic signal (dotted) is at its maximum while the fundamental intensity (solid) is zero. As the displacement increases, it is shown that the second harmonic intensity changes with a period of $\lambda/4$ and the fundamental intensity has a period of $\lambda/2$. Also note that envelopes of the intensity curves decrease gradually due to the Gaussian pulse shape. Because the fundamental signal is much stronger than the harmonic signal, the fundamental intensity in the sum signal would become larger than the second harmonic intensity even when the displacement is small. As shown in Fig. 1, the fundamental signal becomes dominant in the sum signal when the displacement is only 0.02λ. With a typical PRI and realistic tissue motion, the displacement is below $\lambda/8$. In this range, the second harmonic signal monotonically decreases and the fundamental signal monotonically increases.

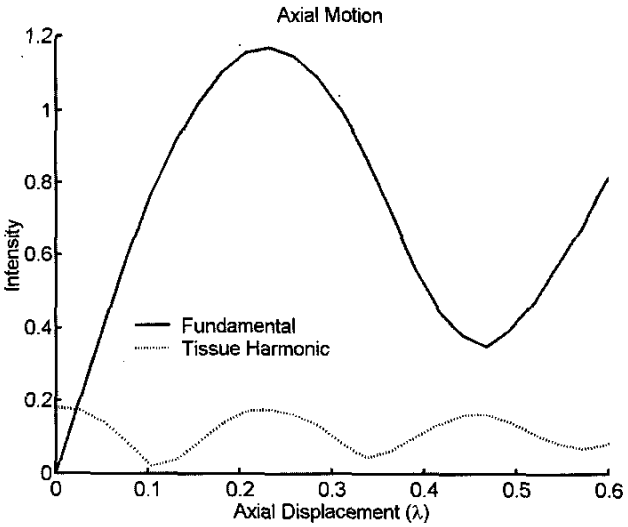

Fig. 1. Signal intensities as a function of axial motion based on simulations. The solid line is the fundamental intensity and the dotted line denotes the tissue harmonic intensity.

For lateral motion, the scatterer is originally positioned at the focal point when the positive pulse arrives. The scatterer then moves laterally between the two pulses. In this case, not only the lateral motion causes a time delay, intensity of the received signal also changes because the scatterer is at a different position within the lateral radiation pattern. In Fig. 2, the horizontal axis represents the lateral displacement (d_{lateral}) normalized to the beam width at the fundamental frequency, and the vertical axis denotes the signal intensities. It is demonstrated that the fundamental signal (solid) increases with the lateral motion as the tissue harmonic intensity (dotted) decreases. It is also shown that the tissue harmonic intensity becomes half of its maximum when the target is out of the acoustic beam. Compared to the axial motion, the harmonic intensity with lateral motion decreases at a relatively slow rate. As shown in Fig. 2, the fundamental intensity becomes larger than the second harmonic intensity when the displacement is larger than 0.3 times the beam width measured at the focal depth. Thus, tissue harmonic imaging is less sensitive to the lateral motion in this case.

When human tissue is imaged, the received ultrasonic signal comes from a collection of scatterers in the sample volume. To investigate the motion artifacts when multiple scatterers are present, speckle signals were also simulated. Signals from ten different scatterer distribution were simulated and analyzed. Each distribution consisted of 100 scatterers randomly positioned around the focal depth. The velocity of tissue motion was assumed to be uniform. In other words, all scatterers moved in the same direction with the same speed. The intensity curve for each distribution was first normalized to its own maximum and the mean and standard deviation of these normalized curves were calculated. The results are shown in Figs. 3 and 4 for axial motion and for lateral motion, respectively. The

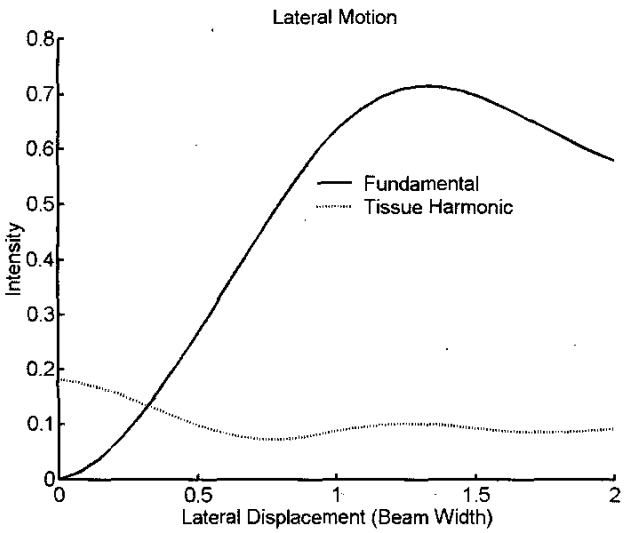

Fig. 2. Signal intensities as a function of lateral motion based on simulations. The solid line is the fundamental intensity and the dotted line denotes the tissue harmonic intensity.

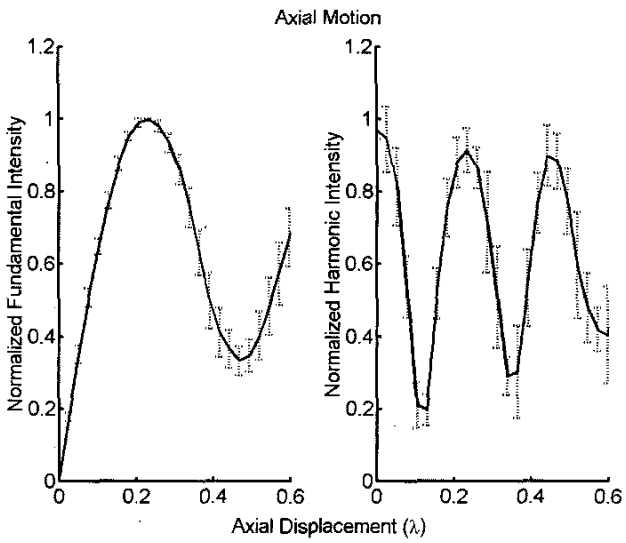

Fig. 3. Simulated signal intensities as a function of axial motion. Multiple scatterers are considered. Left panel: fundamental intensity. Right panel: tissue harmonic intensity.

error bars represent +/− one standard deviation. The left panel of Fig. 3 denotes the fundamental intensity and the right panel shows the harmonic intensity. In both panels, the horizontal axis is the same as that of Fig. 1. It is shown that the intensity curves with multiple scatterers are similar to those with a single scatterer when considering axial motion. For lateral motion, the fundamental intensity curve is also similar to that with a single scatterer. Nevertheless, the harmonic intensity curve is different. Fig. 4 shows that the harmonic intensity does not decrease to half of the maximum as the single scattering case in Fig. 2. It is also noted that the intensity curves with lateral motion have larger variations. This is due to the fact that the lateral motion is more affected by the scatterer distribution within the sample volume.

Experiments were also conducted to investigate the motion effects on signal intensity. A schematic diagram of the experimental setup is shown in Fig. 5. An arbitrary function generator (Gage CompuGen 1100, Montreal, QC, Canada) was used to generate the desired transmit waveform. The transmit waveform was then sent to a power amplifier (Amplifier Research 25A250A, Souderton, PA) to drive a 2.25 MHz focused transducer (Panametrics V304, Waltham, MA). The transducer had a diameter of 29 mm and was geometrically focused at 70 mm. The target was made of a nylon wire with a diameter of 200 μm. A three-axis step motor system (CSI, Taipei, Taiwan, R.O.C.) was used to position the transducer and to control the relative position between the wire target and the transducer. To emulate the target motion, a positive echo was first collected with the target being positioned at the focal point. Then, the transducer was moved step by step and a negative pulse was transmitted at different positions. The received signals were then sent to an ultrasonic receiver (Panametrics Model 5800, Waltham, MA). Finally, an analog-to-digital converter with a 100 Msamples/s sampling rate and 12-bit resolution (Gage CompuScope 12100, Montreal, QC, Canada) was used to sample the signal. For each measurement, the acoustic signal was acquired 32 times for signal averaging. The experimental results are shown in Figs. 6 and 7. Again, the second harmonic intensity decreases with motion while the fundamental intensity increases. The fundamental intensity becomes larger than the harmonic intensity at 0.025λ in Fig. 6 and at 0.2 times the beam width in Fig. 7. The experimental results agree with simulations.

The results in this section indicate that tissue motion has a significant impact on the signal intensity for the PI technique. Axial motion decreases the tissue harmonic intensity whereas the fundamental signal increases. The intensity curves change periodically within the pulse envelope. For lateral motion, the tissue harmonic intensity varies at a relatively slow rate. Because the wavelength and the radiation pattern are related to axial motion and lateral motion respectively, the choice of the transmit frequency affects the sensitivity to motion. In other words, a higher frequency system would be more sensitive to motion due to its shorter wavelength and its narrower radiation pattern. Both simulations and experiments have also indicated that the PI technique is more susceptible to the axial motion than to the lateral motion. Axial motion directly results in a time delay error (i.e., $\tau = 2d_{\text{axial}}/c$) and affects the fundamental signal cancellation due to signal misalignment. However, the time delay error resulted from lateral motion (i.e., $\tau = d_{\text{lateral}}^2/zc$) is not as severe because the image depth z is usually much larger than the lateral displacement. It is also implied that even with the PI technique, a high-pass filter is still required to suppress the fundamental signal if tissue motion cannot be ignored.

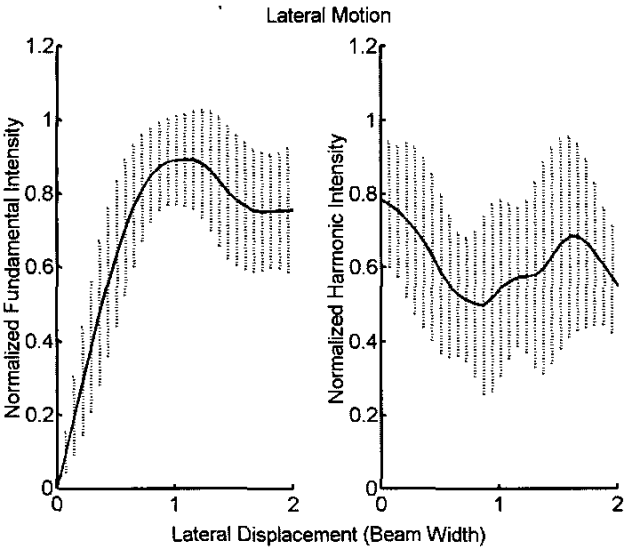

Fig. 4. Simulated signal intensities as a function of lateral motion. Multiple scatterers are considered. Left panel: fundamental intensity. Right panel: tissue harmonic intensity.

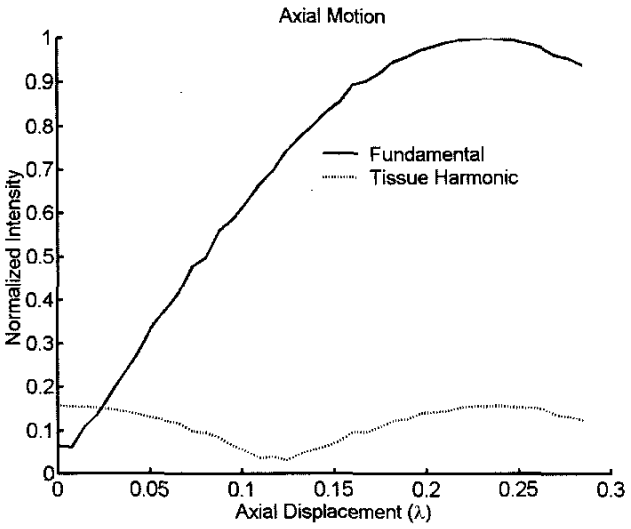

Fig. 6. Measured signal intensities as a function of axial motion. The solid line is the fundamental intensity and the dotted line denotes the tissue harmonic intensity.

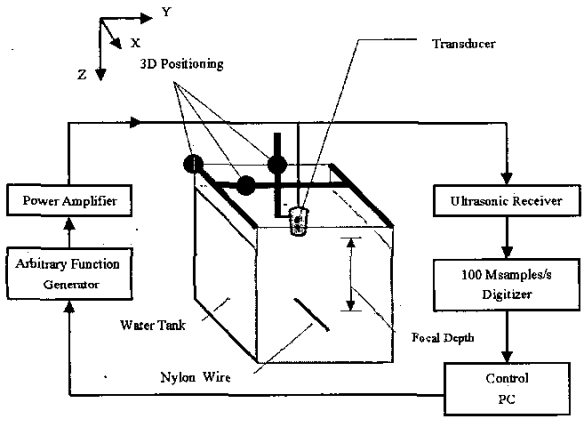

Fig. 5. Schematic diagram of the experiment set-up.

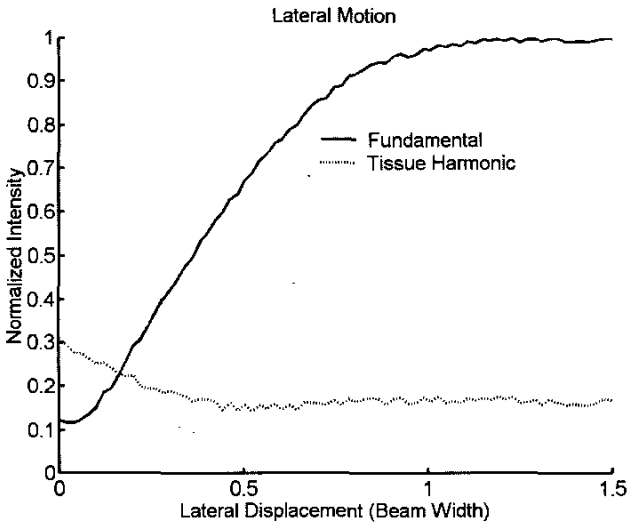

Fig. 7. Measured signal intensities as a function of lateral motion. The solid line is the fundamental intensity and the dotted line denotes the tissue harmonic intensity.

III. Motion and Spectral Leakage

Previous simulations and experimental results have demonstrated that the fundamental intensity increases when the imaged tissue moves. In fact, all linear propagating signals increase due to tissue motion. If the transmit pulse has frequency components in the harmonic bandwidth (i.e., spectral leakage), the leakage signal is not cancelled in the sum. In this case, the harmonic signal consists of two components. One is the desired tissue harmonic signal generated through finite amplitude propagation; the other is the unwanted leakage harmonic signal that is already present prior to acoustic propagation. The leakage signal produces an acoustic beam with different characteristics and significantly affects image quality. As shown in Fig. 8, the solid line represents a typical radiation pattern associated with the tissue harmonic signal and the dotted line denotes a corresponding radiation pattern for the leakage harmonic signal. The sidelobes of the leakage signal are higher compared to those of the tissue harmonic signal. The leakage signal cannot be removed by filtering because it is in the same frequency range as the tissue harmonic signal. Contrast resolution of tissue harmonic imaging is degraded by the high sidelobes due to the uncancelled leakage signal.

Simulations and experiments were performed to evaluate effects of spectral leakage in the presence of tissue motion. All parameters in the simulations are the same as

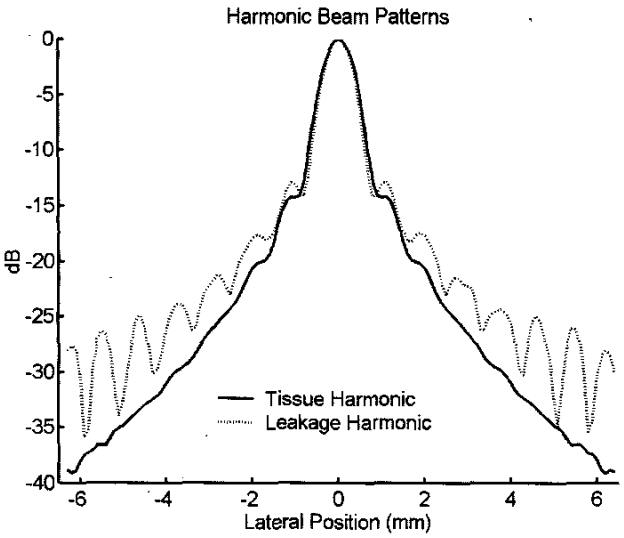

Fig. 8. Simulated tissue harmonic beam pattern (solid) and leakage harmonic beam pattern (dotted).

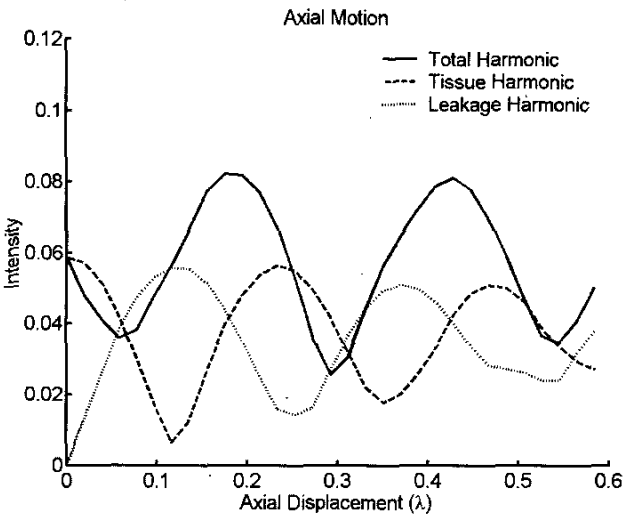

Fig. 9. Simulated signal intensities as a function of axial motion. The solid line is the total harmonic intensity, the dashed line represents the tissue harmonic intensity and the dotted line denotes the leakage signal intensity. The transmit pulse is a gated sine wave.

those used in Section II, except that a 3-cycle sine wave, instead of a Gaussian pulse, was used as the transmit signal. Because the envelope of the gated sine wave is rectangular, considerable leakage is present and it is linearly propagated in the second harmonic band. Fig. 9 shows the simulated harmonic intensities with axial motion. The solid line, the dashed line and the dotted line represent the total harmonic signal, the tissue harmonic signal and the linearly propagated leakage signal, respectively. The leakage harmonic signal is obtained by propagating the transmit waveform linearly, and the total harmonic signal is generated by using nonlinear propagation of the same waveform. In other words, the total harmonic signal consists of a linear signal (i.e., the leakage harmonic signal) and a nonlinear signal (i.e., the tissue harmonic signal).

As shown in Fig. 9, the tissue harmonic intensity and the leakage intensity at the focal depth vary with the axial motion as expected. Compared to the harmonic intensity curves in Fig. 1 (i.e., Gaussian pulse with no significant spectral leakage), the total harmonic intensity curve has significantly different characteristics from the tissue harmonic intensity. Moreover, although the total harmonic intensity may be similar at two different displacements, the corresponding image quality may differ because the composition of the total harmonic signal is not the same. For example, the total harmonic intensity with a displacement of about $\lambda/8$ is almost the same as that with no displacement. However, the leakage signal dominates in the former case while the tissue harmonic signal is the only harmonic signal in the latter case. Similar conclusions can be drawn for lateral motion as shown in Fig. 10. The total harmonic intensity is relatively uniform despite the fact that the intensity curves change significantly for both the tissue harmonic signal and the leakage harmonic signal. Simulated harmonic radiation patterns at the focal depth with different tissue displacement along the axial direction

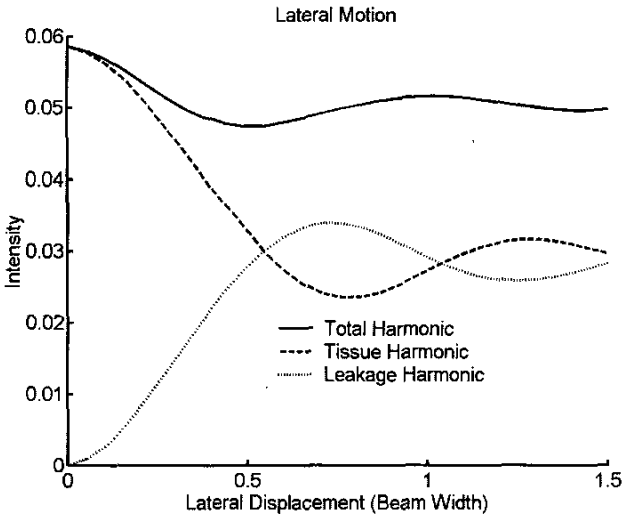

Fig. 10. Simulated signal intensities as a function of lateral motion. The solid line is the total harmonic intensity, the dashed line represents the tissue harmonic intensity and the dotted line denotes the leakage signal intensity. The transmit pulse is a gated sine wave.

are shown in Fig. 11. It is demonstrated that the sidelobes increase due to the leakage signal and the image contrast is degraded when tissue motion is present.

Experiments were also done to investigate the effects on image quality. Acoustic beam patterns in water were measured by a PVDF needle hydrophone (NTR Systems TNU001A, Seattle, WA) with a 30 dB pre-amplifier gain. Position of the hydrophone was controlled by a three-axis step motor system (CSI, Taipei, Taiwan, R.O.C.). The hydrophone had a diameter of 0.6 mm with a flat frequency response from 1 MHz to 20 MHz. The other instruments

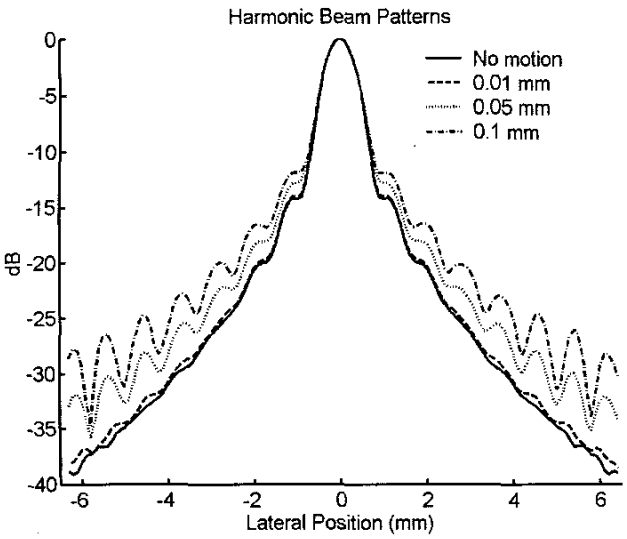

Fig. 11. Simulated harmonic beam patterns with different displacements. Solid line is no motion, dashed line is 0.01 mm, dotted line is 0.05 mm and the dot-dashed line is 0.1 mm.

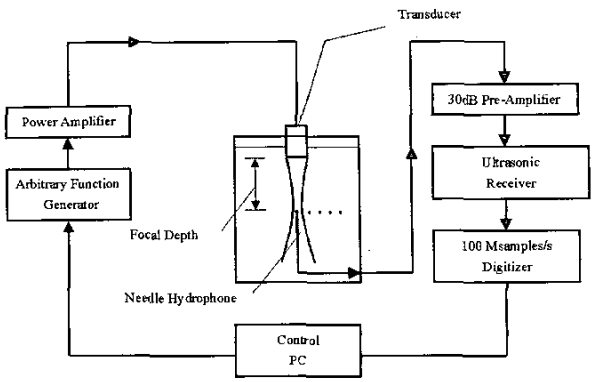

Fig. 12. Schematic diagram of the hydrophone measurement set-up.

are the same as those shown in Fig. 5. A schematic diagram of the experimental setup is shown in Fig. 12. Acoustic beam patterns were sampled in the focal plane with a spacing of 0.5 mm. Because the transducer was circularly symmetric, acoustic beams generated by the transducer were also circularly symmetric. Therefore, only 1-D radial measurements were performed. At each measurement point, the acoustic field was measured 32 times for off-line signal averaging. The experimental results are shown in Fig. 13. The solid line denotes the beam pattern with no motion and the dashed line represents a displacement of 0.01 mm between two firings. The dotted line and the dot-dashed line correspond to displacements of 0.05 mm and 0.1 mm, respectively. It is shown that the motion elevates the sidelobes and thus image quality in tissue harmonic imaging is affected. The faster the target moves, the more degradation is introduced. The experimental results are consistent with previous simulation results.

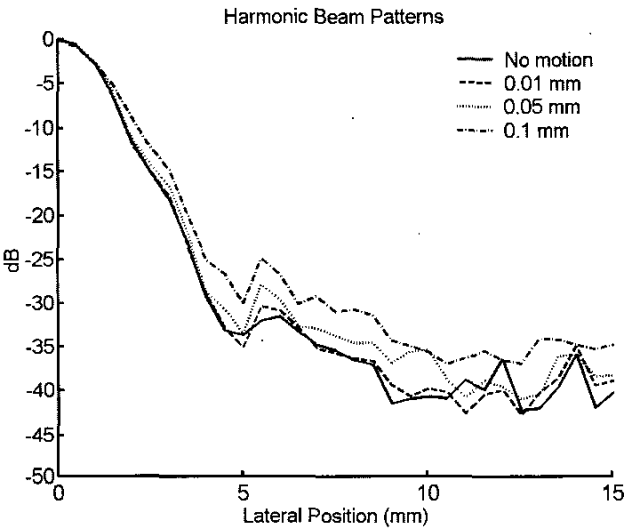

Fig. 13. Measured harmonic beam patterns with different displacements. Solid line is no motion, dashed line is 0.01 mm, dotted line is 0.05 mm and the dot-dashed line is 0.1 mm.

B-scan ultrasonic images were also constructed to demonstrate the contrast degradation due to motion. The experimental setup is the same as that described in Fig. 5 except that a gelatin-based ultrasonic phantom with uniform distribution of glass beads (Sigma G4649, St. Louis, MO) was used as a speckle generating object. An anechoic cyst was created inside the phantom for contrast analysis. The transmit signal was a 1.5 MHz gated sine pulse with a duration of 3 cycles. Five different motions were considered by increasing the axial displacements between the positive pulse and the negative pulse from 0 mm to 0.04 mm. In Fig. 14, results corresponding to displacements of 0 mm, 0.01 mm and 0.03 mm are demonstrated. In the upper panels, spectra of the first scan line are shown and the corresponding B-scan images are illustrated in the lower panels. Spectral leakage is indicated by the elevated fundamental signal level. In Fig. 14, the anechoic cyst is more contaminated by the leakage harmonic signal when the displacement increases. This agrees well with the increase of spectral leakage. Fig. 15 demonstrates the contrast between the anechoic cyst and the background. The contrast is computed from regions inside the two white boxes in each B-scan image. The declining curve indicates that the contrast decreases when the motion increases.

IV. Discussion and Conclusions

In this paper, motion artifacts of PI-based tissue harmonic imaging were investigated using simulations and experiments. It is shown that the tissue harmonic signal is highly susceptible to motion between the transducer and the imaged tissue. With motion, the tissue harmonic signal decreases, and the linear signal increases. The intensity

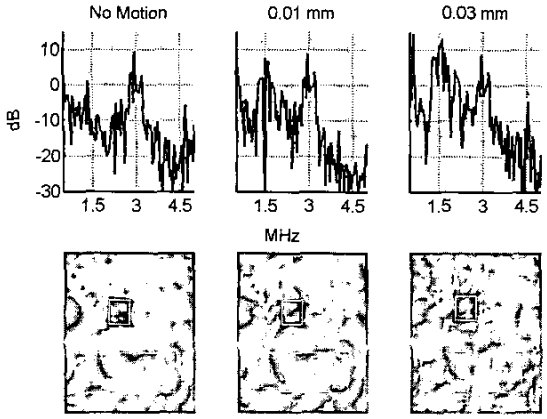

Fig. 14. Spectra and B-scan images with axial displacements of 0 mm, 0.01 mm and 0.03 mm. Upper panels: spectra. Lower panels: B-scan images.

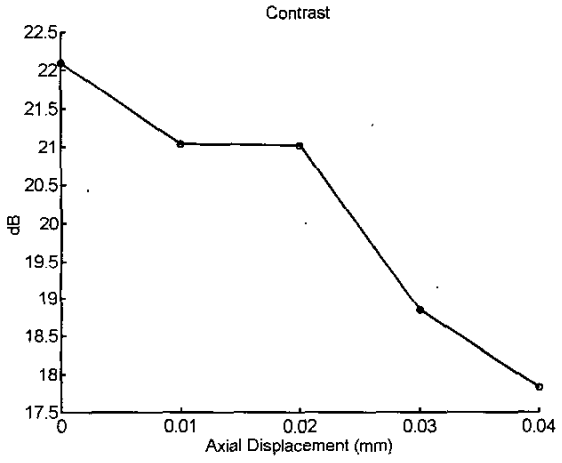

Fig. 15. Image contrast as a function of axial displacement.

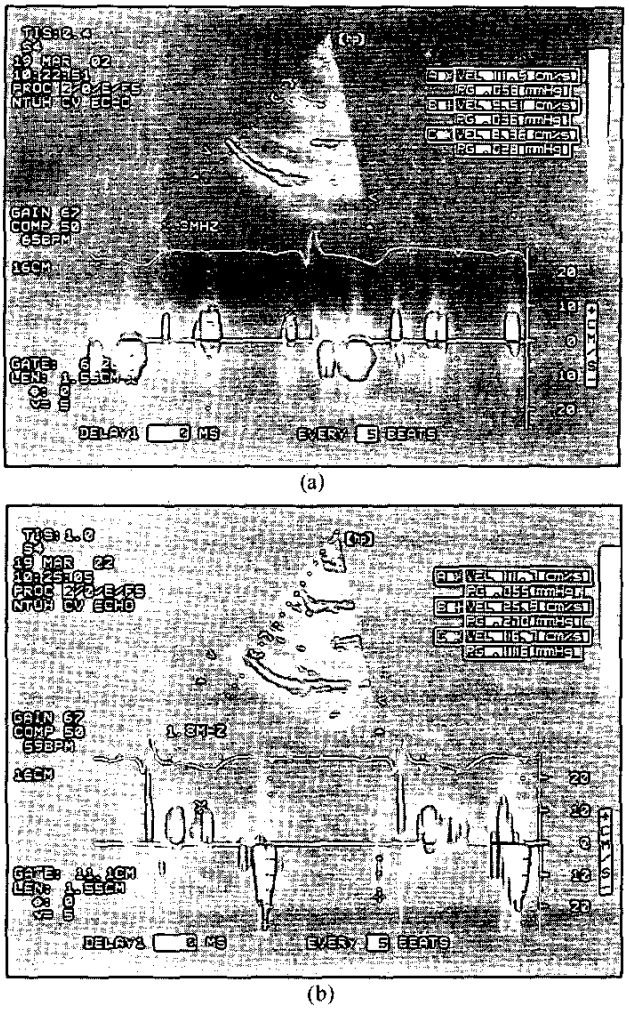

Fig. 16. Tissue Doppler image in PLAX. Doppler gate is positioned on the septum and posterior wall in (a) and (b), respectively. Markers A, B and C correspond to systole, early diastole and late diastole respectively.

generally is more sensitive to axial motion than to non-axial motion. In clinical situations, tissue motion is most pronounced for cardiac imaging. It is less important when imaging stationary or slow moving structures. The myocardial motion was assessed in order to indicate the clinical relevance of the results of this paper. Fig. 16 was acquired in Tissue Doppler mode using a commercial scanner (Hewlett-Packard SONOS 4500, Palo Alto, CA). A healthy young adult at the age of 26 was scanned. The para-sternal long axis view (PLAX) was used. The difference between Fig. 16(a) and (b) is the depth of the Doppler gate. The Doppler gate was positioned on the septum and the posterior wall respectively in Fig. 16(a) and (b). The chamber between the septum and the posterior wall was the left ventricle. In both figures, three markers were used to indicate three different states during a cardiac cycle. Markers A, B and C correspond to ventricular systole, early diastole and late diastole, respectively. At the systole stage, the septum and the wall move inward with a velocity of 11.5 cm/s and 11.7 cm/s. At the early diastole stage, the outward velocity increases to 9.51 cm/s and 25.9 cm/s. The outward velocity then decreases to 8.6 cm/s and 16.7 cm/s at the late diastole stage. In general, the myocardial velocity is about the range from 10 cm/s to 25 cm/s. The velocity range is consistent with that reported in [16]. Based on the typical frequency (1.5 MHz-3.5 MHz) and PRI (200 μs-300 μs) used in cardiac applications, the corresponding displacement could be up to $\lambda/8$. This was also the reason why the displacement between 0 to $\lambda/8$ was of primary concern when the harmonic intensity was discussed in Section II.

As shown in Fig. 1, an axial displacement less than $\lambda/8$ can diminish the tissue harmonic intensity significantly in the sum signal. For lateral motion, the harmonic intensity is less predictable due to the random distribution of scatterers within the sample volume. For both motions, the fundamental signal may increase to a level much higher

than the harmonic signal level for both directions. This indicates that filtering is still required to remove the fundamental signal even though the PI technique was originally developed to cancel the linear signal without the need of filtering. The high-pass filtering inevitably reduces the bandwidth of the tissue harmonic signal because some harmonic signals below the cutoff frequency are rejected. This degrades the axial resolution. Besides, a trade-off between lateral resolution and potential motion artifacts also exists because high frequency signal is more susceptible to motion. Motion artifacts also degrade the contrast resolution in tissue harmonic imaging. The tissue harmonic signal is contaminated by the leakage signal if the linear signal is not cancelled due to motion. In this case, the image contrast is reduced because of the elevated sidelobes.

When tissue inhomogeneities are considered, the intensity curves with lateral motion become more complicated due to the distorted radiation pattern. For axial motion, however, the intensity curves are not affected because both positive and negative pulses suffer from the same phase error. In other words, the effects of tissue inhomogeneities on intensity curves could be ignored when the image object moves in the axial direction. Note that the sidelobe difference between the tissue harmonic beam and the spectral leakage beam differs in the presence of tissue inhomogeneities. The difference decreases when a larger phase error is introduced [8]. In other words, the contrast between the image without motion and the image with motion is reduced in the presence of sound velocity inhomogeneities.

The motion artifacts are even more severe when more firings are used to extract harmonic signals for each beam line. The multiple-firing scheme is also referred to as the phase-coded pulse sequence [17]. For example, a phase-coded pulse sequence with three pulses can be used to extract the third harmonic signal. In this case, phases of the pulses are 0°, 120°, and 240°, respectively. Because the time needed for each sum signal increases, the multiple-firing scheme is more susceptible to motion. Also, the desired third harmonic signal decreases even faster than the second harmonic signal as a function of displacement. However, the pulse inversion Doppler (PID) technique [10] does not directly suffer from the aforementioned intensity variation. This is due to the fact that the positive echo and the negative echo are not summed together to obtain the harmonic signal. Instead, a conventional clutter filter is applied to the Doppler signal.

A simple scheme may be used to correct for the motion artifacts. A correlation-based time shift estimator may be adopted to estimate and compensate for the phase difference introduced by the motion between the positive echo and the negative echo [18]. After motion compensation, the undesired fundamental signal is eliminated and the harmonic signal is restored. Figs. 17 and 18 show the simulated harmonic-to-fundamental ratios with axial motion and lateral motion, respectively. All parameters in the simulations were the same as those used in Section II. The transmit signal was a 2 MHz Gaussian pulse with a −6 dB 50% fractional bandwidth and the f/number in the simulations was 2. The harmonic-to-fundamental ratio is defined as the ratio of the harmonic intensity to the fundamental intensity. The higher the ratio, the more effective motion compensation is. The ratio is the highest with no displacement. In this case, only tissue harmonic signal remains and the ratio is infinite. It is shown that, when the axial motion is considered, the correction scheme effectively improves the harmonic-to-fundamental ratio. As shown in Fig. 18, however, little improvement is obtained with lateral motion correction. This is because the simple correlation-based method only accounts for axial motion. Because the 1-D correlation-based method generally does not estimate the lateral motion, 2-D motion correction is required.

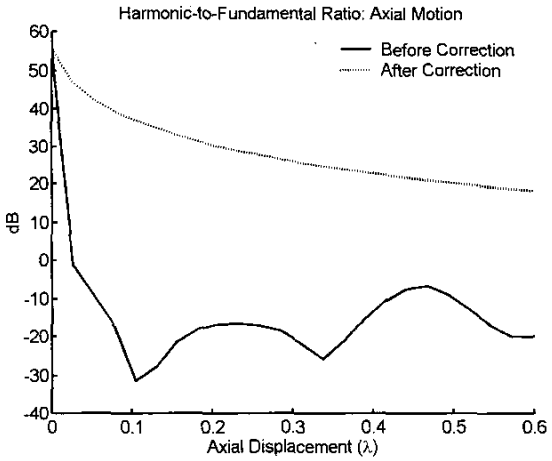

Fig. 17. Harmonic-to-fundamental ratio for axial motion correction. The solid line corresponds to the ratio before correction and the dotted line is the ratio after correction.

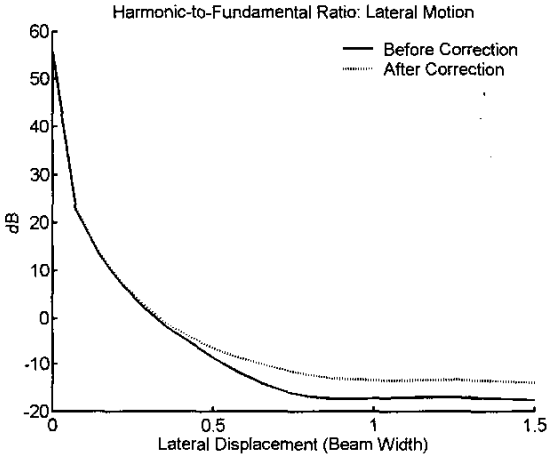

Fig. 18. Harmonic-to-fundamental ratio for lateral motion correction. The solid line corresponds to the ratio before correction and the dotted line is the ratio after correction.

ACKNOWLEDGMENT

The authors thank Dr. Lin at the National Taiwan University Hospital for getting the cardiac images and the reviewers for insightful comments.

REFERENCES

[1] T. Christopher, "Finite amplitude distortion-based inhomogeneous pulse echo ultrasonic imaging," *IEEE Trans. Ultrason., Ferroelect., Freq. Contr.*, vol. 44, no. 1, pp. 125–139, Jan. 1997.

[2] T. Christopher, "Experimental investigation of finite amplitude distortion-based second harmonic pulse echo ultrasonic imaging," *IEEE Trans. Ultrason., Ferroelect., Freq. Contr.*, vol. 45, no. 1, pp. 158–162, Jan. 1998.

[3] P.-C. Li and C.-C. Shen, "Effects of transmit focusing on finite amplitude distortion based second harmonic generation," *Ultrason. Imag.*, vol. 21, pp. 243–258, 1999.

[4] F. Tranquart, N. Grenier, V. Eder, and L. Pourcelot, "Clinical use of ultrasound tissue harmonic imaging," *Ultrasound Med. Biol.*, vol. 25, no. 6, pp. 889–894, 1999.

[5] C. A. Cain, "Ultrasonic reflection mode imaging of the nonlinear parameter B/A: I. A theoretical basis," *J. Acoust. Soc. Amer.*, vol. 80, no. 1, pp. 28–32, July 1986.

[6] R. T. Beyer and S. V. Letcher, *Nonlinear Acoustics*. New York: Academic, 1969.

[7] M. E. Haran and B. D. Cook, "Distortion of finite amplitude ultrasound in lossy media," *J. Acoust. Soc. Amer.*, vol. 73, no. 3, pp. 774–779, Mar. 1983.

[8] C.-C. Shen and P.-C. Li, "Harmonic leakage and image quality degradation in tissue harmonic imaging," *IEEE Trans. Ultrason., Ferroelect., Freq. Contr.*, vol. 48, no. 3, pp. 728–736, May 2001.

[9] D. H. Simpson and P. N. Burns, "Pulse inversion doppler: A new method for detecting nonlinear echoes from microbubble contrast agents," in *Proc. IEEE Ultrason. Symp.*, 1997, pp. 1597–1600.

[10] D. H. Simpson, C. T. Chin, and P. N. Burns, "Pulse inversion doppler: A new method for detecting nonlinear echoes from microbubble contrast agents," *IEEE Trans. Ultrason., Ferroelect., Freq. Contr.*, vol. 46, no. 2, pp. 372–382, Mar. 1999.

[11] P. Jiang, Z. Mao, and J. C. Lazenby, "A new harmonic imaging scheme with better fundamental frequency cancellation and higher signal-to-noise ratio," in *Proc. IEEE Ultrason. Symp.*, 1998, pp. 1589–1594.

[12] D. L. Liu and R. C. Waag, "Propagation and backpropagation for ultrasonic wavefront design," *IEEE Trans. Ultrason., Ferroelect., Freq. Contr.*, vol. 44, pp. 1–12, Jan. 1997.

[13] J. W. Goodman, *Introduction to Fourier Optics*. New York: McGraw-Hill, 1968.

[14] P. T. Christopher and K. J. Parker, "New approaches to nonlinear diffractive field propagation," *J. Acoust. Soc. Amer.*, vol. 90, no. 1, pp. 488–499, July 1991.

[15] W. K. Law, L. A. Frizzell, and F. Dunn, "Determination of the nonlinearity parameter B/A of biological media," *Ultrasound Med. Biol.*, vol. 11, no. 2, pp. 307–318, 1985.

[16] K. Shan, R. J. Bick, B. J. Poindexter, S. Shimoni, G. V. Letsou, M. J. Reardon, J. F. Howell, W. A. Zoghbi, "Relation of tissue doppler derived myocardial velocities to myocardial structure and beta-adrenergic receptor density in humans," *J. Am. Coll.*, vol. 3, pp. 891–896, Sep 2000.

[17] W. Wilkening, M. Krueger, and H. Ermert, "Phase-coded pulse sequence for non-linear imaging," in *Proc. IEEE Ultrason. Symp.*, 2000, pp. 1597–1600.

[18] L. F. Nock and G. E. Trahey, "Synthetic receive aperture imaging with phase correction for motion and for tissue inhomogeneities, Part I: Basic principles," *IEEE Trans. Ultrason., Ferroelect., Freq. Contr.*, vol. 39, no. 4, pp. 489–495, July 1992.

Che-Chou Shen was born in 1976 in Taiwaon, R.O.C. He graduated from the Department of Electrical Engineering at National Taiwan University in 1998. He is now a Ph.D. student working on ultrasonic harmonic imaging under the instruction of Professor P.-C. Li.

Pai-Chi Li (S'91–M'93–S'93–M'95–SM'01) received the B.S. degree in electrical engineering from National Taiwan University, Taipei, Taiwan, R.O.C., in 1987, and the M.S. and Ph.D. degrees from the University of Michigan, Ann Arbor, in 1990 and 1994, respectively, both in electrical engineering: systems.

Dr. Li was a research assistant with the Department of Electrical Engineering and Computer Science at the University of Michigan from 1990 to 1994. He joined Acuson Corporation, Mountain View, CA, as a member of the technical staff in June 1994. His work with Acuson was primarily in the areas of medical ultrasonic imaging system design for both cardiology and general imaging applications. In August 1997, he returned to the Departmentof Electrical Engineering at National Taiwan University as an assistant professor. He became an associate professor in August 1998. His current research interests include biomedical ultrasonoic imaging and signal processing.

He is a senior member of IEEE, and he was the recipient of the Distinguished Achievement Award in Electrical Engineering: Systems for his outstanding academic achievement at the University of Michigan.